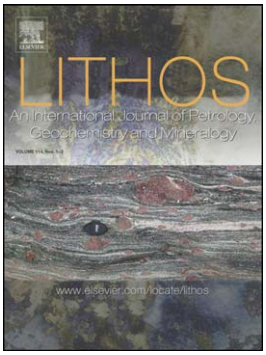

Garnet effect on Nd-Hf isotope decoupling: Evidence from the Jinfosi batholith, Northern Tibetan Plateau

Hui Huang, Yaoling Niu, Xuanxue Mo

PII: S0024-4937(16)30460-1
DOI: doi:10.1016/j.lithos.2016.12.025
Reference: LITHOS 4186

To appear in: *LITHOS*

Received date: 22 September 2016
Accepted date: 21 December 2016

Please cite this article as: Huang, Hui, Niu, Yaoling, Mo, Xuanxue, Garnet effect on Nd-Hf isotope decoupling: Evidence from the Jinfosi batholith, Northern Tibetan Plateau, *LITHOS* (2016), doi:10.1016/j.lithos.2016.12.025

Garnet effect on Nd-Hf isotope decoupling: Evidence from the Jinfosi batholith, Northern Tibetan Plateau

Hui Huang[1*, 2], **Yaoling Niu**[1, 3*, 4], **Xuanxue Mo**[1]

[1] *School of Earth Science and Mineral Resources, China University of Geosciences, Beijing, 100083, China*

[2] *Isotope Laboratory, Department of Earth and Space Sciences, University of Washington, Seattle, WA 98195-1310, USA*

[3] *Department of Earth Sciences, Durham University, Durham, DH1 3LE, UK*

[4] *Institute of Oceanology, Chinese Academy of Sciences, Qingdao 266071, China*

Submitted to _*Lithos*___

Corresponding authors:

Dr. Hui Huang (hui.huang.geo@gmail.com)

Professor Yaoling Niu (yaoling.niu@foxmail.com)

ABSTRACT

The initial Nd and Hf isotope ratios of a 420 Ma post-collisional dioritic-granitic batholith from the northern Tibetan plateau define a negative trend above and orthogonal to the $\varepsilon_{Hf}(t)$-$\varepsilon_{Nd}(t)$ terrestrial array. This uncommon trend offers an insight into the origin of the puzzling Nd-Hf isotope decoupling in the crustal rocks. On this trend, samples depleted in heavy rare earth elements (HREEs, i.e., $[Dy/Yb]_N >>1$) deviate most from the terrestrial array whereas samples with flat HREEs (i.e., $[Dy/Yb]_N \geq 1$) deviate less or plot within the terrestrial array, pointing to the controlling effect of garnet in the magma source. Ancient garnet-bearing residues after melt extraction will have elevated Lu/Hf ratios and can evolve with time to produce high $\varepsilon_{Hf}(t)$ at a low $\varepsilon_{Nd}(t)$ value. Mixing of melts derived from such source lithologies (high Lu/Hf) with melts possessing a within-terrestrial array Nd-Hf isotopic composition (low Lu/Hf) best explains the observed trend orthogonal to the terrestrial array. The samples from the Jinfosi batholith with the most decoupled Nd-Hf isotope compositions require a larger degree (>40%) and ancient (i.e., ≥1.8 Gyr) previous melt extraction from their source. It follows that the ancient melts with depleted HREEs complementary to those garnet-bearing residues should have low ε_{Hf} values and plot below the terrestrial array, which is indeed shown by some Archean/Paleoproterozic TTGs.

Key words: garnet effect; Nd-Hf isotope decoupling; TTG; the North Qilian Orogenic Belt

INTRODUCTION

Extensive isotopic studies of mantle and crustal rocks over the past decades have led to the wide perception that Lu-Hf and Sm-Nd isotopic systems behave in a similar fashion during magmatic processes, leading to the globally correlated terrestrial array in the ε_{Nd}–ε_{Hf} space (Salters and Hart, 1991; Vervoort and Patchett, 1996; Chauvel et al., 2008). Nevertheless, Nd-Hf isotopic decoupling has been documented and discussed in many mantle-derived rocks (Salters and Zindler, 1995; Bizimis et al., 2003; Nowell et al., 2004). The Nd-Hf isotopic decoupling in the crustal environment is expected, but this has not been well recognized. Garnet is a unique major phase that can significantly fractionate Lu/Hf and Sm/Nd ratios in the crust (Vervoort and Patchett, 1996). This is because garnet preferentially retains Lu over Hf without significantly fractionating Sm from Nd during magmatism (Green et al., 2000), i.e., $Kd_{Lu/Hf}^{garnet} \gg 1$ and $Kd_{Sm/Nd}^{garnet} \geq 1$. The dominant mechanism of crustal anatexis usually leaves garnet as a residual phase in the deep crust. The residual garnet has elevated Lu/Hf with moderate Sm/Nd, resulting in much more rapid ingrowth of radiogenic Hf compared to Nd. Consequently, lower crustal rocks and many granitoids generated by reworking of the ancient lower crust are expected to have time-integrated Nd-Hf isotopic decoupling. Indeed, Schmitz et al. (2004) reported significant present-day Nd-Hf isotopic decoupling in lower crust granulites. In some subduction-related rocks, e.g. slab-derived adakites, Nd-Hf isotopic decoupling has also been observed (Polat and Münker, 2004). However, these studies suggested a metamorphic origin for the Nd-Hf isotopic decoupling (Schmitz et al., 2004) and greater fluid mobility of Nd or Hf during metamorphism (Polat and Münker, 2004).

The expected "garnet effect" on lower crustal rocks in terms of the Nd-Hf decoupling, however, appears to be rare and remains unclear (Vervoort and Patchett., 1996; Vervoort et al., 2000). This is partly because most Hf isotope data in the study of crustal rocks are largely zircon *in situ* analyses rather than whole rock data (It is common that *in situ* ε_{Hf} values in different zircons from single samples can have > 10-unit variation at a given whole rock ε_{Nd}), and partly because most crustal granitoids or their sources are too young to develop anomalous Hf isotope ratios (Vervoort and Patchett., 1996).

Here, we report our Nd-Hf isotopic study of a post-collisional felsic-intermediate sample suite in a 420 Ma Jinfosi batholith from the Northern Tibetan Plateau. The negative slope of our data plotted above and orthogonal to the terrestrial array in the $\varepsilon_{Hf}(t)$-$\varepsilon_{Nd}(t)$ space offers a novel perspective on Nd-Hf isotopic decoupling as the result of the presence and effect of garnet in granitoid sources of ancient age.

GEOLOGICAL BACKGROUND

The North Qilian Orogenic Belt (NQOB), Qilian Block (QB) and North Qaidam ultrahigh pressure metamorphic belt (NQ-UHPM) form the Qilian Orogenic belt (QOB) on the northern Tibetan Plateau (Fig. 1, Song et al., 2006). The Mohe gneiss within the NQ-UHPM is the oldest sampled crystalline basement in the QOB, dated at ~ 2.5 Ga (Li et al., 2007), and the inherited zircons with ages >2.6 Ga confirm the existence of an Archean basement in the region (Huang et al., 2015; 2016). Different models have been proposed to explain the tectonic evolution in the whole QOB (Xu et al., 1994; Yin and Harrison, 2000; Yang et al., 2002; Gehrels et al., 2003, 2011; Song et al., 2006, 2013, 2014; Wu et al., 2006, 2010; Xu Z. Q, 2006; Xiao et al., 2009; Huang et al., 2015). The

most recent comprehensive studies suggest that the NQOB, QB and NQ-UHPM are different products corresponding to one convergence event, during which the subduction was initiated at ~520 Ma, the ocean basin was closed at 440 Ma, exhumation happened around ~ 420-400 Ma and final orogen collapsed at ~360 Ma (Song et al., 2006, 2009, 2013, 2014; Wang et al., 2014). In this model, the NQOB is considered to be an oceanic suture zone, the QB represents an imbricate thrust belt, and the NQ-UHPM represents a continental-type subduction zone.

The Jinfosi batholith is one of the largest batholiths in the NQOB, considered as typical products of intra-crustal differentiation in a syn/post-collisional setting (Hu et al., 2006; Zhang et al., 1995; Wu et al., 2010; Song et al., 2013). The NQOB consists of ophiolites, metamorphic rocks and arc magmatic sequences. The magmatic rocks are dominated by calc-alkaline intermediate-felsic volcanic rocks and I-type granitoids with ages of 516 to 446 Ma (Wang et al., 2005; Chen et al., 2014), generally coupled with the subduction-related HP metamorphic activities (489-440 Ma) (Wu et al., 1993; Zhang et al., 1997, 2007; Song et al., 2004, 2006; Liu et al., 2006). The Jinfosi batholith is ~ 60 km long and 10-12 km wide, extending in NW-direction in the northwestern part of the NQOB (Fig. 1, Song et al., 2013). The batholith intruded the Ordovician back-arc basin volcanic complex and the Silurian sedimentary sequence. It mainly consists of peraluminous granite, biotite monzonite, and minor diorite (Zhang et al., 1995; Hu et al., 2006; Wu et al., 2010; Song et al., 2013). Major minerals include varying amounts of quartz (Qtz), K-feldspar (Kfs), plagioclase (Pl), biotite (Bt), muscovite, tourmaline and

garnet (Grt). Zircon U-Pb dating using the SHRIMP method yields a weighted mean U-Pb age of 424±3 Ma (Wu et al., 2010).

METHODS

Samples were carefully cleaned for analysis of major elements, trace elements and whole rock Sr-Nd-Pb-Hf isotopes. All the detailed analytical details are given in Huang et al. (2014). Here is a brief description. Whole rock Sr, Nd, Pb and Hf isotope analyses were conducted on a Thermo Finnigan Neptune Plasma Ionisation Multi-collector Mass Spectrometer (PIMMS) instrument in the Northern Centre for Isotopic and Elemental Tracing (NCIET) at Durham University. Sr-Nd-Pb-Hf isotopic analyses were carried out during different analytical sessions for each isotope. The international standards NBS987, J&M, NBS981 and JMC475 were used for Sr, Nd, Pb and Hf isotopes, respectively. The long term performance of the Neptune PIMMS at Durham University for Sr, Nd and Hf isotopes was reported by Nowell et al. (2003). The Sr standard NBS987 yield average $^{87}Sr/^{86}Sr$ of 0.710277 ± 0.000020 (2SD, n = 39). All data are normalized relative to the accepted standard $^{87}Sr/^{86}Sr$ ratios for NBS 987 of 0.71024 (Thirlwall, 1991). The average $^{143}Nd/^{144}Nd$ of J&M is 0.511107 ± 0.000012 (2SD, n = 47). All data are normalized relative to the accepted standard $^{143}Nd/^{144}Nd$ ratio for J&M of 0.511110 (Thirlwall, 1991). The average of Hf standard JMC475 is 0.282145±0.000008 (2SD, n=37). Corrections for isobaric interferences from Yb and Lu on ^{176}Hf were made by monitoring ^{173}Yb and ^{175}Lu. All data are normalized relative to the accepted standard $^{176}Hf/^{177}Hf$ ratio for JMC475 of 0.28216 Nowell et al. (1998). For Pb, mass bias was corrected using $^{205}Tl/^{203}Tl$ ratios and an exponential law. The best fit ratio for all the Pb ratios was determined for each

analytical session by minimizing the difference in offset between all Pb ratios and the Galer (1999) values.

Laser ablation ICP-MS zircon U-Pb analysis was carried on an Agilent 7500 ICP-MS instrument equipped with a GeoLas 2005 at China University of Geosciences, Wuhan. Detailed operating conditions for the laser ablation system and ICP-MS instrument and data reduction are the same as described by Liu et al. (2008). Zircon 91500 was used as the external standard and analyzed twice every 5 samples. Standard silicate glass NIST610 was used to optimize the instrument. Common Pb was corrected by ComPbCorr#3_17 (Andersen, 2002). Age calculations and Concordia plots were made using isoplot (Ludwig, 2003). The obtained mean $^{206}Pb/^{238}U$ ages for 91500 and GJ-1 are 1062.3±1.3 Ma (2σ, n=202) and 599.7±1.2 Ma (2σ, n=60), respectively. These results are consistent with the recommended values (Wiedenbeck et al., 1995; Jackson et al., 2004).

RESULTS

The minerals in samples from the Jinfosi batholith in this study include Bt, Pl, Kfs and Qtz with Bt varying from 5% to 20%. Some of the samples are peraluminous granites while others are more mafic and chemically equivalent to diorites, corresponding to a broad SiO_2 range of 56.8-72.5 wt% with A/CNK 0.9~1.1 (Table S1). The enclosed amphibolite xenoliths (QL10-01) are foliated mafic diorite, containing amphibole (Amp), Bt, Pl and Qtz. Major element data, trace element data and zircon U-Pb dating results are presented as supplements. Whole rock Sr-Nd-Hf-Pb isotopes are given in Table 1. The Nd-Hf isotope data plotted in Figures are initial values ($\varepsilon_{Nd}(t)$, $\varepsilon_{Hf}(t)$), calculated using the zircon U-Pb age. Most zircons yield concordant or slightly

discordant U-Pb ages (Fig. 2). The results indicate that the intrusion was emplaced in the early Triassic ~ 424 Ma (Fig. 2), consistent with previous work (Wu et al., 2010). Inherited zircons yield age populations of 450-500 Ma and 1.0 Ga (Fig. 2), reflecting the earlier magmatic events in the region (Wu et al., 2010; Song et al., 2013; Huang et al., 2015). The presence of a discordant age of ~1.4 Ga is indicative of inheritance from old lithologies.

Whole rock analyses clearly indicate the Nd-Hf isotopic decoupling had occurred prior to the petrogenesis of the batholith. This is demonstrated by initial Nd and Hf isotopes which define a negative trend displaced above and orthogonal to the terrestrial array in the ε_{Hf}-ε_{Nd} space (Fig. 3). Samples (QL10-05, QL10-08) with higher Dy/Yb values and distinctively depleted heavy rare earth elements (HREEs) have highest $\varepsilon_{Hf}(t)$ values (Fig. 4). Other samples with lower Dy/Yb values and flat HREEs have relatively lower $\varepsilon_{Hf}(t)$ values (Fig. 4), and plot progressively closer to the terrestrial array (Fig. 3). We note that the $\varepsilon_{Nd}(t)$ values display a positive correlation with MgO, while the $\varepsilon_{Hf}(t)$ values show an unexpected negative correlation (Fig. 5). These opposing correlations indicate that the Nd-Hf isotopic decoupling is caused by the anomalous behaviour of Hf isotopes. The enclosed xenolith plots off the trend defined by the host samples and also has an unusually high $\varepsilon_{Hf}(t)$ for a given $\varepsilon_{Nd}(t)$ (Figs. 3, 5B). The samples exhibit limited variations in their initial Pb isotopes (Pb_i) ($^{208}Pb/^{204}Pb_i$=38.35–38.61, $^{207}Pb/^{204}Pb_i$=15.66–15.74, $^{206}Pb/^{204}Pb_i$=17.94 – 19.16, Table 1) and initial Sr isotopic ratios (I_{Sr} = 0.705 to 0.708, Table 1).

DISCUSSION

Source constraints

Our samples have a large compositional range in SiO_2 (57-72 wt%). The most felsic sample QL10-05 (72% SiO_2) may share some "S-type" features and others have "andesitic" (or "dioritic") compositions. Given the peraluminous nature of some samples in this study, sediment effect on Nd-Hf isotopic decoupling should be considered (Patchett et al., 1984; Chauvel et al., 2008). The present-day sedimentary materials generally have elevated ε_{Hf} at a given ε_{Nd} (Chauvel et al., 2008), but this is not adequate to explain the Nd-Hf isotopic decoupling we observe. There are three reasons. (1) Metasedimentary rocks have negative ε_{Hf} values at 420 Ma and more negative if they are more ancient (ε_{Nd}<-15, ε_{Hf}<-10, Chauvel, et al. 2008), while the most felsic sample QL10-05 with the most decoupled Nd and Hf isotopes have $\varepsilon_{Hf}(420)$ of 12.8 and $\varepsilon_{Nd}(420)$ of -6.5. (2) Sedimentary rocks have highly radiogenic Sr isotopes ($I_{Sr} \cong 0.718$, Plank and Langmuir 1998) while QL10-05 has I_{Sr} of 0.704. (3) Sedimentary rocks are generally heterogeneous, but S-type-like granites with decoupled Nd-Hf isotopes are rarely sampled. Specifically, in the Qilian region, other S-type-like batholiths do not show Nd-Hf isotopic decoupling (Huang et al., 2015; Yang et al., 2016). Compared to the two-mica granites (Yang et al., 2016) and S-type granitoids (Huang et al., 2015) in other Qilian Batholiths, I_{Sr} values in this study are less radiogenic (0.705 to 0.708 vs. >0.710), $\varepsilon_{Nd}(t)$ values are higher (-4 to -2 v.s. -12.2 to -3.4) and $\varepsilon_{Hf}(t)$ values are much higher (-3.4 to 12.8 v.s. -12 to 3.4). Lead isotopes are consistent with the Pb isotopic compositions of the regional crystalline basement (Zhang et al., 1995; Chen et al., 2007). Thus, the isotopic data indicate limited contributions from highly enriched upper crust.

It is possible that samples with high SiO_2 and depleted HREEs result from elevated accumulation of quartz and feldspars (Wang et al., 2013) or are caused by garnet and amphibole separation at an early evolution stage. However, the decoupling in our samples are initial values, and fractional crystallization can not produce variations in the initial isotopic signature.

The Jinfosi samples display large Nd-Hf isotopic heterogeneity and decoupling. Disequilibrium melting of zircon during crustal anatexis could generate Hf isotope heterogeneity (Tang et al., 2014). But zircon is a minor phase in the crust, and it is difficult to explain the decoupling against the observed general correlation of HREE-depletion with high $\varepsilon_{Hf}(t)$. Garnet, as the most important HREE host phase, has the potential to cause the Nd-Hf isotopic decoupling. To melt the garnet-bearing lower crust, three scenarios are possible. First, if garnet breaks down during crustal anatexis, the derivative melt would have elevated HREEs and ε_{Hf}, which is not mirrored in our study. Second, if garnet does not break down but does not equilibrate with the melt, the derivative melt would have low HREEs and low ε_{Hf}. Third, if garnet does not break down and equilibrates with the melt in the garnet stability field, the derivative melt will have low HREE and elevated ε_{Hf}. Our samples with elevated ε_{Hf} and depleted HREEs are consistent with the scenario of equilibrium melting with garnet being a residual phase.

The interpretation of these data is complicated by the fact that the variation in initial values can reflect source characteristics, crustal contamination, and magma mixing. However, a common and essential factor in these models is the incorporation of a component that has a substantially decoupled Nd-Hf isotopic composition. It is important to note that the samples with Nd-Hf isotopes that plot furthest away from the terrestrial

array are most depleted in the HREEs with higher Dy/Yb values, while samples with Nd-Hf isotopes plotting close to or within the terrestrial array have flat HREEs with lower Dy/Yb values (Figs. 4). This is a simple manifestation of the "garnet effect".

Modelling

It is possible to model the involvement of garnet in the generation of the strongly decoupled Nd-Hf isotope compositions in the Jinfosi samples. To explore such processes, we use equilibrium melting to illustrate possible Nd and Hf isotope evolution trends as a result of partial melting a lower crust with garnet being a residual phase. If the Jinfosi magma derived from such a source had involved assimilation or mixing processes, then the measured ε_{Hf} values would be minima. Hence, our modelling only provides the conservative estimate.

The ages of ~ 2.5 Ga, 2.0 Ga and 1.8 Ga correspond to important episodes of regional continental crust growth (Grimmer et al., 2003; Tung et al., 2007, 2008). Therefore, the different curves in Fig. 3 represent the loci of isotopic compositions of the residual lower crust with previous melt extraction at 2.5, 2.0 and 1.8 Ga, respectively, calculated at the emplacement age (420 Ma) of the Jinfosi batholith. Re-melting these residua at 420 Ma will pass on the isotope features to the derivative Jinfosi magma. In our calculation, the 2.5Ga Mohe basement was used as a representative regional lower crust composition (Chen et al., 2007; Li et al., 2007). It is reasonable to use such an old basement because the appearance of the discordant U-Pb age of ~1.4 Ga indicates the inheritance from old lithologies.

To illustrate the concept in detail, a few possible mineral assemblages during crustal anatexis (Rapp, 1991; 1995; Vervoort and Patchett, 1996) are examined and only minerals with great potential to cause fractionations between Lu-Hf and Sm-Nd systems are considered. Sources of granitoid magmatism are mostly mafic to intermediate rocks. Therefore, partition coefficients were chosen for a mafic lower crust source. Values are from Vervoort and Patchett (1996) who made the pioneering effort to model the effect of garnet on Nd-Hf isotopic decoupling in the lower crust environment. The results are summarized in Fig. 3. For the given extent of melting and residual mineral modes, the greatest Nd-Hf isotope decoupling is coupled with older (more ancient) melt extraction/depletion (pink vs blue, orange curves in Fig. 3). The ingrowth of radiogenic Hf isotopes also increases with increasing residual garnet mode (changes along the curve, Fig. 3), with increasing extent of melting (solid line vs dashed line in Fig. 3) and with decreasing Cpx/Pl ratio (numerical ratios in Fig. 3). The Cpx/Pl= 1:2 curves slightly bend back to the terrestrial array at garnet modes >30% (Fig. 3) because of the slightly decreasing Lu/Hf ratios resulting from different extents of Lu-Hf growth in the modelling. Re-melting of these ancient melting residues at 420 Ma will produce melts with depleted HREEs and inherited signatures of Nd-Hf isotope decoupling as manifested by the 420 Ma Jinfosi granitic samples. In Fig. 3, the sample with the most decoupled Nd-Hf isotopes at lowest ε_{Nd} value is close to the 2.0 Ga and 2.5 Ga curve. Its isotopic compositions are consistent with a residue produced by 40% melting at 2.5Ga with 15% garnet and a 1:2 ratio of Cpx to Pl (Fig. 3). It can also be explained by re-melting a residue produced by 50% partial melting at 2.0 Ga with 30% residual garnet and a 1:2 ratio of Cpx to Pl (Fig. 3). Melt depletion younger than 1.8 Ga or melting degrees lower

than 40% (50%, only if depletion occurred after 2.0 Ga) will produce residues with Nd-Hf isotopes that plot within the terrestrial array in Fig. 3A. Although the calculation may seem simplistic and limited given the possible complexities involved in crustal melting, it adequately demonstrates that a large extent of melting (>40 %) can effectively fractionate Lu-Hf from Sm-Nd system, and that long residence time is required to ensure that the residues evolve to the isotopic characteristics inherited by the Jinfosi granitic samples.

The amphibolite xenolith also shows decoupled Nd-Hf isotopes with Hf isotopes similar to those of the Jinfosi plutonic samples, but the Nd isotopic ratios of the amphibolite is more radiogenic than those of the Jinfosi plutonic samples (Fig. 3, Fig. 5B). It is unlikely that this xenolith is cognate to the Jinfosi magma because the amphibolite has distinct mineralogy, texture and isotopic compositions (Barbarin, 2005; Huang et al., 2014). We interpret the xenolith as being country rock captured during magma emplacement. The presence of this xenolith provides evidence that the Nd-Hf isotopic decoupling may be common in the regional lower crust.

The global database for the lower crust shows that a few samples have super chondritic Lu/Hf ratios that have potential to evolve out of the terrestrial array (Vervoort et al., 2000). These studies suggest the possibilities of finding significantly decoupled Nd-Hf isotopes in granitic magmas derived by melting of the lower crust. However, such granitoids appear to be rare. It is highly likely that the sources from which these granitoids were derived may have had melt depletion too recently to have developed significant Nd-Hf isotope decoupling. Vervoort and Patchett (1996) estimated that hundreds of millions years are required for a garnet-bearing residue to evolve off the terrestrial array. Indeed, our modelling specifically requires that the time-integrated

evolution must be longer than 1.4 Gyrs (=1.8 Ga - 420 Ma). Additionally, a large extent of melting (≥ 40%) is also necessary for significant radiogenic Hf in-growth and thus enhances Nd-Hf isotope decoupling. This is because, in addition to the garnet effect, Lu/Hf in the melting residues increases with increasing extent of melting. 40-50% is unusually high and perhaps it points to the unusual thermal conditions during the petrogenesis of the Jinfosi magma and also accounts for the rarity of such magmas with anomalous Nd-Hf isotopes. Such a large degree of partial melting may be rare; but it is possible that prior to 1.8 Ga larger amounts of partial melting occurred given the greater internal heat at that time (Rapp et al., 1991, 1995; Peacock, 1994). For example, 20-40% melting of mafic lower crust can result in granitic melts; 50-60% melting can result in more andesitic/mafic melts (Rapp et al., 1991, 1995). However, residues after such high degrees of partial melting may be too refractory to melt again unless there is an additional heat supply. In the case of the NQOB, this is feasible in the context of post-collisional extension (~ 420-400 Ma), where basaltic melt derived from upwelling hot asthenospheric mantle could have underplated the crust and caused melting of ancient residual crust. The most straightforward way to explain the Jinfosi sample trend is to mix such basalts with mantle array Nd-Hf isotope compositions with melts of lower crust with decoupled Nd-Hf isotopes. This is also supported by the broad negative correlation between $\varepsilon_{Hf}(t)$ and MgO (Fig. 5B) which suggests that samples with higher MgO have lower $\varepsilon_{Hf}(t)$ while samples with lower MgO have higher $\varepsilon_{Hf}(t)$. There are other equally mathematically valid models that can be applied too. For example, it is possible that an andesitic magma with normal Nd-Hf isotopes assimilates the highly isotopically decoupled lower-crust. Alternatively, the Jinfosi sample suite may reflect a series of

magmas derived at different pressures involving different amounts of residual garnet, i.e., above the garnet-stability field (flat HREEs) and within the garnet stability field (depleted HREEs). In this case, it requires different degrees of partial melting accordingly to explain the negatively correlated $\varepsilon_{Hf}(t)$-MgO trend (Fig. 4). Nevertheless, in all these situations, a key component with HREE-depletion and decoupled Nd-Hf isotopes ("garnet effect") is required.

The evidence for occurrence of a garnet effect in the lower crust is limited by the nature of sampling (Schmitz et al., 2004). Extraction of melt within the garnet stability field will lead to garnet-bearing residua that evolve rapidly with time, above the mantle Nd-Hf isotope array. The complementary melts should evolve below the array. Possible examples are tonalite–trondhjemite–granodiorite (TTG) suites, which dominate the preserved Archean crustal masses (Condie, 1981; Martin et al., 2005; Hoffmann et al., 2011). The TTGs were produced by 20-40% melting at depths where garnet was present as a residual phase (Rapp et al., 1991; Rapp and Watson, 1995; Xiong, 2006). The longer crustal residence of TTGs promotes greater evolution and divergence in their isotope compositions. It is thus expected that the ancient TTGs have present-day Nd and Hf isotopes below the terrestrial array. We have compiled the available Nd-Hf isotope data for the TTGs of Archean and Proterozoic age (Fig. 6). Indeed, many of them plot below the terrestrial array as anticipated. Some of the TTGs plot within the array, reflecting the complexities of the TTGs petrogenesis, e.g., some of them may be derived through multiple partial melting events or a lower extent of melting, and/or lower modal garnet in the melting residues as evidenced by the abundant TTGs with flat HREEs.

ACKNOWLEDGEMENT

The research was supported by Chinese NSFC grants (91014003, 41130314, 41503007) and Chinese Academy of Sciences Innovation (Y42217101L). Grants from Shandong Province and City of Qingdao are also appreciated. We thank Prof. Michael Roden and Prof. Shuguang Song for the constructive comments. Thanks are owed to Editor Sun-Lin Chung for editorial help. In addition Prof. Michael Roden, Professor Jean-François Moyen, Prof. Paterno Castillo, and three anonymous reviewers provided insightful comments that helped to improve the early version of this manuscript.

REFERENCES

Andersen, T., 2002. Correction of common lead in U–Pb analyses that do not report ^{204}Pb. Chemical Geology, 192, 59–79.

Barbarin, B., 2005. Mafic magmatic enclaves and mafic rocks associated with some granitoids of the central Sierra Nevada batholith, California: nature, origin, and relations with the hosts. Lithos 80, 155-177.

Bizimis, M., Sen, G., Salters, V.J.M., 2003. Hf–Nd isotope decoupling in the oceanic lithosphere: constraints from spinel peridotites from Oahu, Hawaii. Earth and Planetary Science Letters 217, 43-58.

Chauvel, C., Lewin, E., Carpentier, M., Arndt, N. T., Marini, J. C. 2008. Role of recycled oceanic basalt and sediment in generating the Hf–Nd mantle array. Nature geoscience 1(1), 64-67.

Chen, N.S., Wang, X.Y., Zhang, H.F., Sun, M., Li, X.Y., Chen, Q., 2007. Geochemistry and Nd-Sr-Pb Isotopic Compositions of Granitoids from Qaidam and Oulongbuluke Micro-Blocks，NW China Constraints on Basement Nature and Tectonic Affinity. Journal of Earth Science 32, 7–21.

Chen, Y.X., Song, S.G., Niu, Y.L., Wei, C.J., 2014. Melting of continental crust during subduction initiation: A case study from the Chaidanuo peraluminous granite in the North Qilian suture zone. Geochimica Et Cosmochimica Acta 132, 311-336.

Condie, K.C., 1981. Archean greenstone belts. Elsevier.

Galer, S.J., 1999. Optimal double and triple spiking for high precision lead isotopic measurement. Chemical Geology, 157(3): 255- 274.

Gehrels, G., Kapp, P., DeCelles, P., Pullen, A., Blakey, R., Weislogel, A., Ding, L., Guynn, J., Martin, A., McQuarrie, N., 2011. Detrital zircon geochronology of pre-Tertiary strata in the Tibetan-Himalayan orogen. Tectonics 30, TC5016.

Gehrels, G.E., Yin, A., Wang, X.F., 2003. Magmatic history of the northeastern Tibetan Plateau. Journal of Geophysical Research 108, 2423.

Green, T.H., Blundy, J.D., Adam, J., Yaxley, G.M., 2000. SIMS determination of trace element partition coefficients between garnet, clinopyroxene and hydrous basaltic liquids at 2–7.5 GPa and 1080–1200°C. Lithos 53, 165-187.

Grimmer, J.C., Ratschbacher, L., McWilliams, M., Franz, L., Gaitzsch, I., Tichomirowa, M., Hacker, B.R., Zhang, Y., 2003. When did the ultrahigh-pressure rocks reach the surface? A $^{207}Pb/^{206}Pb$ zircon, $^{40}Ar/^{39}Ar$ white mica, Si-in-white mica, single-grain provenance study of Dabie Shan synorogenic foreland sediments. Chemical Geology 197, 87-110.

Hoffmann, J.E., Münker, C., Polat, A., Rosing, M.T., Schulz, T., 2011. The origin of decoupled Hf–Nd isotope compositions in Eoarchean rocks from southern West Greenland. Geochimica et Cosmochimica Acta 75, 6610-6628.

Hu, N.G., Su, J.P., Zhang, H.F., Feng, B.Z., 2006. Geochemical characteristics and petrogenesis of Jinfosi pluton in Qilian Mountains. Journal of Earth Sciences and Environment 28, 5-12 (in Chinese with English abstract).

Huang, H., Niu, Y.L., Nowell, G., Zhao, Z., Yu, X., Zhu, D., Mo, X., Ding, S., 2014. Geochemical constraints on the petrogenesis of granitoids in the East Kunlun Orogenic Belt, Northern Tibetan Plateau: implications for the continental crust growth through syncollisional felsic magmatism. Chemical Geology, 370, 1-18.

Huang, H.,Y.L. Niu, G. Nowell, Z.D. Zhao, X.H. Yu, X.X. Mo. 2015. The nature and history of the Qilian Block in the context of the development of the Greater Tibetan Plateau, Gondwana Research, 28, 209-224.

Huang, H., Niu, Y. and Mo, X., 2016. Syn-collisional granitoids in the Qilian Block on the Northern Tibetan Plateau: A long-lasting magmatism since continental collision through slab steepening. Lithos, 246, 99-109.

Jackson, S.E., Pearson, N.J., Griffin, W.L., Belousova, E.A., 2004. The application of laser ablation-inductively coupled plasma-mass spectrometry to in situ U–Pb zircon geochronology. Chemical Geology 211, 47-69.

Li, X.Y., Chen, N.S., Xia, X.P., Sun, M., Xu, P., Wang, Q.Y., Wang, X.Y., 2007. Constraints on the timing of the early-Paleoproterozoic magmatism and crustal evolution of the Oulongbuluke microcontinent: U-Pb and Lu-Hf isotope systematics of zircons from Mohe granite pluton. Acta Petrologica Sinica 23, 513−522. (In Chinese with English abstract).

Liu, Y.J., Neubauer, F., Genser, J., Takasu, A., Ge, X.-H., Handler, R., 2006. $^{40}Ar/^{39}Ar$ ages of blueschist facies pelitic schists from Qingshuigou in the Northern Qilian Mountains, western China. Island Arc 15, 187-198.

Liu, Y.S., Hu, Z.C., Gao, S., Gunther, D., Xu, J., Gao, C.G., Chen, H.H., 2008. *In situ* analysis of major and trace elements of anhydrous minerals by LA-ICP-MS without applying an internal standard. Chemical Geology 257 (1-2), 34-43.

Ludwig, K.R., 2003. A geochronological toolkit for microsoft excel. Isoplot, 3, 1-70.

Martin, H., Smithies, R.H., Rapp, R., Moyen, J.F., Champion, D., 2005. An overview of adakite, tonalite–trondhjemite–granodiorite (TTG), and sanukitoid: relationships and some implications for crustal evolution. Lithos 79, 1-24.

Nowell, G.M., Pearson, D.G., Bell, D.R., Carlson, R.W., Smith, C.B., Kempton, P.D., Noble, S.R., 2004. Hf Isotope Systematics of Kimberlites and their Megacrysts: New Constraints on their Source Regions. Journal of Petrology 45, 1583-1612.

Nowell, G. et al., 1998. High precision Hf isotope measurements of MORB and OIB by thermal ionisation mass spectrometry: insights into the depleted mantle. Chemical Geology, 149(3), 211□233.

Nowell, G.M., Parrish, R.R., 2001. Simultaneous acquisition of isotope compositions and parent/daughter ratios by non□isotope dilution solution□mode plasma ionisation multi□collector mass spectrometry (PIMMS). Plasma Source Mass Spectrometry: The New Millennium. Royal Society of Chemistry, Special Publication, 267, 298□310.

Nowell, G.M., Pearson, D.G., Ottley, C.J., Schweiters, J., Dowall, D., 2003. Long□term performance characteristics of a plasma ionisation multi□collector mass spectrometer (PIMMS): the ThermoFinnigan Neptune. Plasma Source Mass Spectrometry: Applications and Emerging Technologies. Cambridge: Royal Society of Chemistry: 307□320.

Patchett, P., White, W., Feldmann, H., Kielinczuk, S., Hofmann, A., 1984. Hafnium/rare earth element fractionation in the sedimentary system and crustal recycling into the Earth's mantle. Earth and Planetary Science Letters 69, 365-378.

Peacock, S.M., Rushmer, T. and Thompson, A.B., 1994. Partial melting of subducting oceanic crust. Earth and planetary science letters, 121(1), 227-244.

Plank, T. and Langmuir, C.H., 1998. The chemical composition of subducting sediment and its consequences for the crust and mantle. Chemical geology 145(3), 325-394.

Polat, A., Münker, C., 2004. Hf–Nd isotope evidence for contemporaneous subduction processes in the source of late Archean arc lavas from the Superior Province, Canada. Chemical Geology 213, 403-429.

Rapp, R.P., Watson, E.B., 1995. Dehydration melting of metabasalt at 8–32 kbar: Implications for continental growth and crust-mantle recycling. Journal of Petrology 36, 891-931.

Rapp, R.P., Watson, E.B., Miller, C.F., 1991. Partial melting of amphibolite/eclogite and the origin of Archean trondhjemites and tonalites. Precambrian Research 51, 1-25.

Salters, V.J.M., Hart, S.R., 1991. The mantle sources of ocean ridges, islands and arcs: the Hf-isotope connection. Earth and Planetary Science Letters 104, 364-380.

Salters, V.J.M., Zindler, A., 1995. Extreme $^{176}Hf/^{177}Hf$ in the sub-oceanic mantle. Earth and Planetary Science Letters 129, 13-30.

Schmitz, M.D., Vervoort, J.D., Bowring, S.A., Patchett, P.J., 2004. Decoupling of the Lu-Hf and Sm-Nd isotope systems during the evolution of granulitic lower crust beneath southern Africa. Geology 32, 405.

Shan, H., Zhai, M., Wang, F., Zhou, Y., Santosh, M., Zhu, X., Zhang, H., Wang, W., 2015. Zircon U–Pb ages, geochemistry, and Nd–Hf isotopes of the TTG gneisses from the Jiaobei terrane: Implications for Neoarchean crustal evolution in the North China Craton. Journal of Asian Earth Sciences 98, 61-74.

Song, S., Zhang, L., Niu, Y., Song, B., Zhang, G., Wang, Q., 2004. Zircon U-Pb SHRIMP ages of eclogites from the North Qilian Mountains in NW China and their tectonic implication. Chinese Science Bulletin 49, 848-852.

Song, S., Zhang, L., Niu, Y., Su, L., Song, B., Liu, D. 2006. Evolution from oceanic subduction to continental collision: a case study from the Northern Tibetan Plateau

based on geochemical and geochronological data. Journal of Petrology 47(3), 435-455.

Song, S.G., Niu, Y.L., Zhang, L.F., Zhang, G.B., 2009. Time constraints on orogenesis from oceanic subduction to continetnal subduction, collision, and exhumation: an example from North Qilian and North Qaidam HP-UHP belts. Acta petrologica Sinica 25, 2067-2077.

Song, S., Niu, Y., Su, L., Xia, X., 2013. Tectonics of the North Qilian orogen, NW China. Gondwana Research 23, 1378-1401.

Song, S., Niu, Y., Su, L., Zhang, C., Zhang, L., 2014. Continental orogenesis from ocean subduction, continent collision/subduction, to orogen collapse, and orogen recycling: The example of the North Qaidam UHPM belt, NW China. Earth-Science Reviews 129, 59-84.

Sun, S.s., McDonough, W.F., 1989. Chemical and isotopic systematics of oceanic basalts: implications for mantle composition and processes. Geological Society, London, Special Publications 42, 313-345.

Tang, M., Wang, X.-L., Shu, X.-J., Wang, D., Yang, T., Gopon, P., 2014. Hafnium isotopic heterogeneity in zircons from granitic rocks: Geochemical evaluation and modeling of “zircon effect” in crustal anatexis. Earth and Planetary Science Letters 389, 188-199.

Thirlwall, M.F., 1991. Long□term reproducibility of multicollector Sr and Nd isotope ratio analysis. Chemical Geology: Isotope Geoscience section, 94(2), 85□104.

Tung, K.A., Yang, H.J., Yang, H.Y., Liu, D.Y., Zhang, J.X., Wan, Y.S., Tseng, C.Y., 2007. SHRIMP U-Pb geochronology of the zircons from the Precambrian basement of the Qilian Block and its geological significances. Chinese Science Bulletin 52, 2687-2701.

Tung, K.A., Yang, H.R., Yang, H.Y., Liu, D.Y., et al., 2008. Qilian Neoproterozoic granitoids SHRIMP zircon U-Pb geochronology, elemental and Sr - Nd isotope geochemistry. Bulletin of mineralogy, petrology and geochemistry 27, 106-108.

Vervoort, J.D., Jonathan Patchett, P., 1996. Behavior of hafnium and neodymium isotopes in the crust: Constraints from Precambrian crustally derived granites. Geochimica et Cosmochimica Acta 60, 3717-3733.

Vervoort J. D., Patchett P. J., Blichert-Toft J., Albarede F.,1999. Relationships between Lu–Hf and Sm–Nd isotopic systems in the global sedimentary system. Earth Planet. Sci. Lett. 168, 79–99.

Vervoort, J.D., Jonathan Patchett, P, Albarede, F., Blichert-Toft, J. et al., 2000. Hf-Nd isotopic evolution of the lower crust. Earth and Planetary Science Letters, 181, 115-129.

Vervoort, J. D., Plank, T., Prytulak, J. 2011. The Hf–Nd isotopic composition of marine sediments. Geochimica et Cosmochimica Acta,75(20), 5903-5926.

Wang, C.Y., Zhang, Q., Qian, Q., Zhou, M.F., 2005. Geochemistry of the Early Paleozoic Baiyin volcanic rocks (NW China): implications for the tectonic evolution of the North Qilian orogenic belt. The Journal of geology 113, 83-94.

Wang, M.J., Song, S.G., Niu, Y.L., Su, L., 2014. Post-collisional magmatism: Consequences of UHPM terrane exhumation and orogen collapse, N. Qaidam UHPM belt, NW China. Lithos 210, 181-198.

Wang, S.J., Li, S.G., Chen, L.J., He, Y.S., An, S.C. and Shen, J., 2013. Geochronology and geochemistry of leucosomes in the North Dabie Terrane, East China: implication for post-UHPM crustal melting during exhumation. Contributions to Mineralogy and Petrology, 165(5), 1009-1029.

Wiedenbeck, M., Alle, P., Corfu, F., Griffin, W., Meier, M., Oberli, F., Quadt, A.v., Roddick, J., Spiegel, W., 1995. Three natural zircon standards for U‐Th‐Pb, Lu‐Hf, trace element and REE analyses. Geostandards newsletter 19, 1-23.

Wu, C.L., Yao, S.Z., Zeng, L.S., al., E., 2006. Double subduction of the Early Paleozoic North Qilian oceanic plate: evidence from granites in the central segment of North Qilian, NW China. Geology in China 33, 1197-1208 (in Chinse with English abstract).

Wu, C.L., Xu, X.Y., Gao, Q.M., Li, X.M., Lei, M., et al., 2010. Early Palaezoic granitoid magmatism and tectonic evolution in North Qilian, NW China. Acta Petrologica Sinica 26, 1027-1044 (in Chinese with English abstract).

Wu, H.Q., Feng, Y.M., Song, S.G., 1993. Metamorphism and deformation of blueschist belts and their tectonic implications, North Qilian Mountains, China. Journal of Metamorphic Geology 11, 523-536.

Xiao, W.J., Windley, B.F., Yong, Y., Zhen, Y., Chao, Y., Liu, C.Z., Li, J., 2009. Early Paleozoic to Devonian multiple-accretionary model for the Qilian Shan, NW China. Journal of Asian Earth Sciences 35, 323-333.

Xiong, X.-L., 2006. Trace element evidence for growth of early continental crust by melting of rutile-bearing hydrous eclogite. Geology 34, 945.

Xu Z. Q, Y.J.S., Li H. B., Zhang J.X., Zeng L. S., Jiang M., 2006. The Qinghai-Tibet plateau and continental dynamics: a review on terrain tectonics, collisional orogenesis, and processes and mechanisma for the rise of the plateau. Geology in China 33, 221-238.

Xu, Z.q., Xu, H.f., Zhang, J.x., al., e., 1994. The Zoulang Nanshan Caledonian Subduction Complex in the Northern Qilian Mountains and Its Dynamics1. Acta Geologica Sinica- English Edition 7, 225-241.

Yang, J.S., Xu, Z.Q., Zhang, J.X., Song, S.G., Wu, C.L., Shi, R.D., Li, H.B., Maurice, B., 2002. Early Palaeozoic North Qaidam UHP metamorphic belt on the north-eastern Tibetan plateau and a paired subduction model. Terra Nova 14, 397-404.

Yang, J.-H., Wu, F.-Y., Wilde, S.A., Zhao, G., 2008. Petrogenesis and geodynamics of Late Archean magmatism in eastern Hebei, eastern North China Craton: Geochronological, geochemical and Nd–Hf isotopic evidence. Precambrian Research 167, 125-149.

Yang, H., Zhang, H., Luo, B., Gao, Z., Guo, L., & Xu, W. 2016. Generation of peraluminous granitic magma in a post-collisional setting: A case study from the eastern Qilian orogen, NE Tibetan Plateau. Gondwana Research,36, 15-32.

Yin, A., Harrison, T.M., 2000. Geologic evolution of the Himalayan-Tibetan Orogen. Ann. Rev. Earth Planet. Sci 28, 211-280.

Zhang, D.Q., Sun, G.Y., Xu, H.L., 1995. Petrology and Isotope Chronology of the Jinfosi Pluton，Qilian Mts., Gansu. Acta Geoscientia Sinica 37, 375-385.

Zhang, J., Xu, Z., Chen, W., Xu, H., 1997. A tentative discussion on the ages of the subduction–accretionary complex/volcanic arcs in the middle sector of North Qilian Mountain. Acta Petrologica et Mineralogica 16, 112-119.

Zhang, J.X., Meng, F.C., Wan, Y.S., 2007. A cold Early Palaeozoic subduction zone in the North Qilian Mountains, NW China: petrological and U-Pb geochronological constraints. Journal of Metamorphic Geology 25, 285-304.

FIGURE CAPTIONS

Fig. 1, A, Schematic map showing major tectonic units of the Qilian Orogenic Belt (after (Song et al., 2013)). B, Simplified geological map of the North Qilian Orogenic Belt (NQOB; after Song et al., 2013).

Fig. 2. Zircon U-Pb Concordia diagrams to show the age of Jinfosi batholith.

Fig. 3, initial whole rock $\varepsilon_{Nd}(t)$- $\varepsilon_{Hf}(t)$ values of Jinfosi samples and modelling results of $\varepsilon_{Nd}(t)$- $\varepsilon_{Hf}(t)$ values at 420 Ma for residues produced by melting lower continental crust (LCC) at 2.5 Ga, 2.0 Ga and 1.8 Ga, respectively. The amphibolite xenolith plots off the sample trend. Global terrestrial array (grey field) is from Vervoort et al. (1999). Qilian Block juvenile granitoids are given for reference (Huang et al., 2015). Ticks on each line represent increasing residual garnet percentages from left to right at a given clinopyroxene to plagioclase ratio (Cpx:Pl). Cpx to Pl ratios are assumed to be 1:2, 1:1 and 2:1, after Vervoort and Patchett (1996). Grt proportions are set from 10% to 50%. Hf isotope data for Mohe basement are from Li et al. (2007). Nd isotope data for Mohe basement are from Chen et al. (2007). F: Melt fraction.

Fig. 4A, $\varepsilon_{Hf}(t)$-Dy/Yb plot to show that samples with higher Dy/Yb ratios have higher $\varepsilon_{Hf}(t)$ values and that samples with lower Dy/Yb ratios have lower $\varepsilon_{Hf}(t)$ values. Fig. 4B, chondrite-normalized rare earth element plots (Sun and McDonough, 1989).

Fig. 5A, Positive correlation between ε_{Nd} and MgO. 4B, negative correlation between ε_{Hf} and MgO, suggesting the anomalous behaviour in Hf isotopes. Big arrows do not include the xenolith.

Fig. 6, Compilation of present day Nd-Hf isotopic compositions for Archean-Paleoproterozoic TTGs showing that they plot below the terrestrial array due to equilibration with residual garnet, compared to the melting residues with above mantle-array Nd-Hf isotopes. Vectors are estimated according to Fig. 3. Data are from Hoffmann et al. (2011), Shan et al. (2015), Yang et al. (2008). Terrestrial array is from Vervoort et al. (2011).

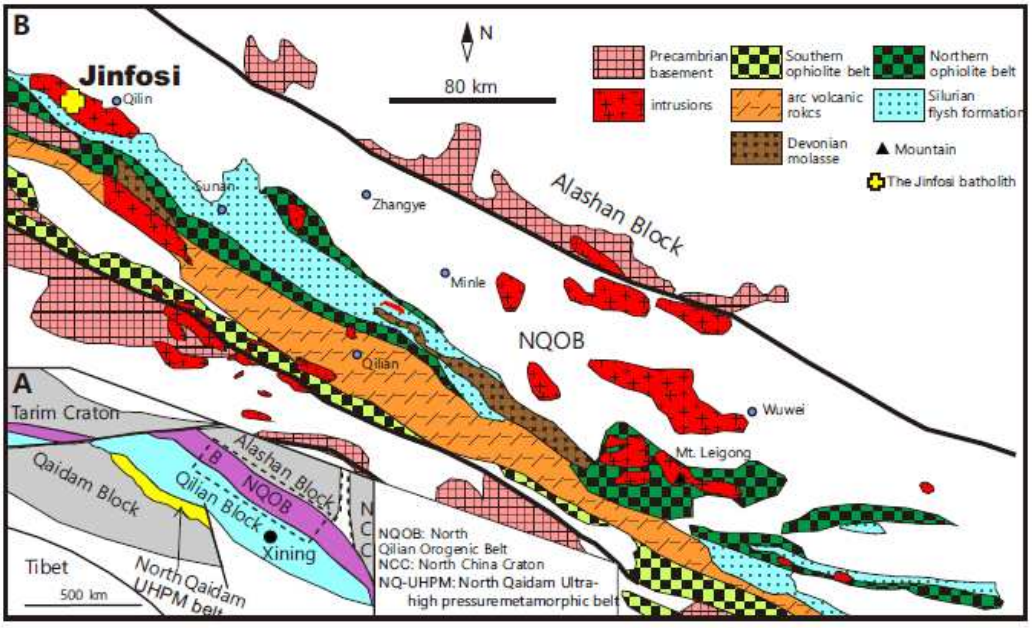

Fig. 1

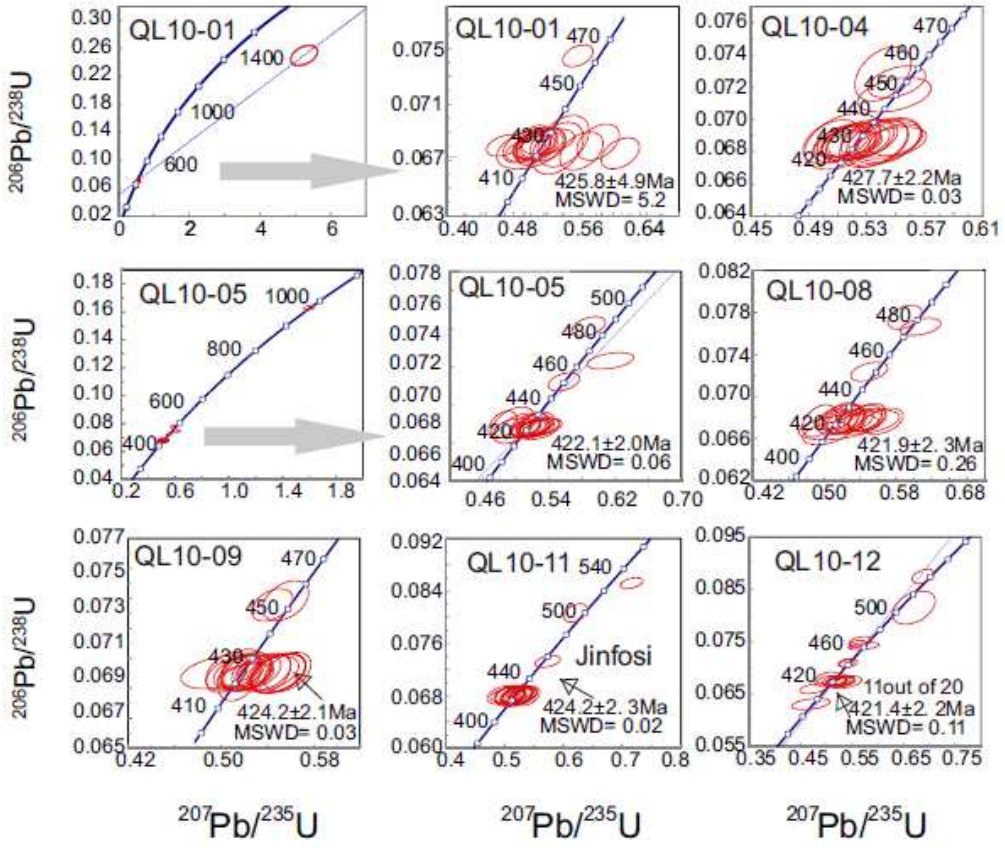

Fig. 2

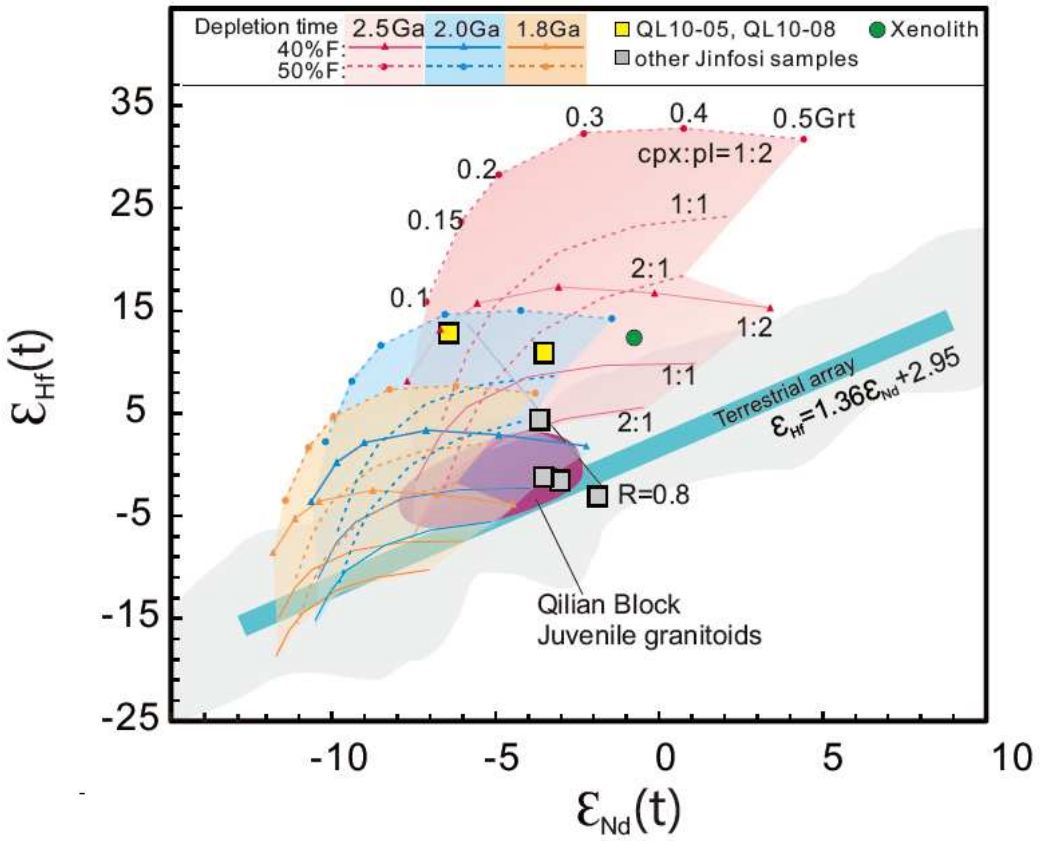
Depletion time 2.5Ga 2.0Ga 1.8Ga
40%F:
50%F:
QL10-05, QL10-08
Xenolith
other Jinfosi samples
0.3
0.4
0.5Grt
cpx:pl=1:2
0.2
1:1
0.15
2:1
0.1
1:2
1:1
2:1
R=0.8
Terrestrial array
$\varepsilon_{Hf}=1.36\varepsilon_{Nd}+2.95$
Qilian Block
Juvenile granitoids
$\varepsilon_{Hf}(t)$
$\varepsilon_{Nd}(t)$
35
25
15
5
-5
-15
-25
-10
-5
0
5
10

Fig. 3

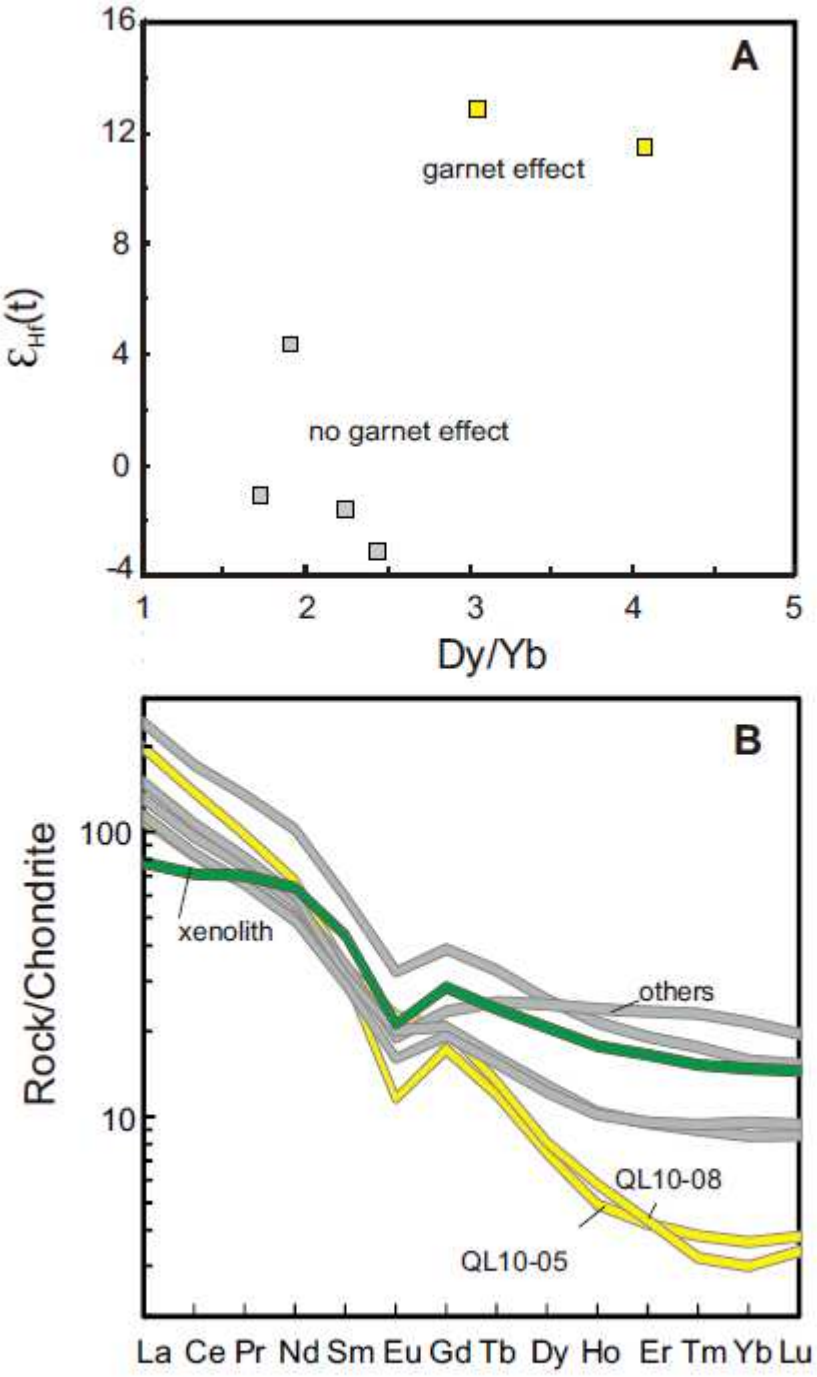

Fig.4

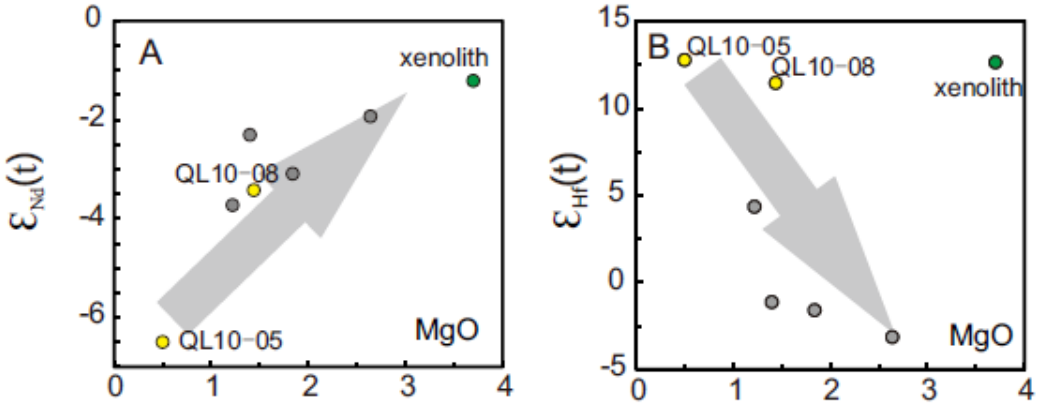

Fig. 5

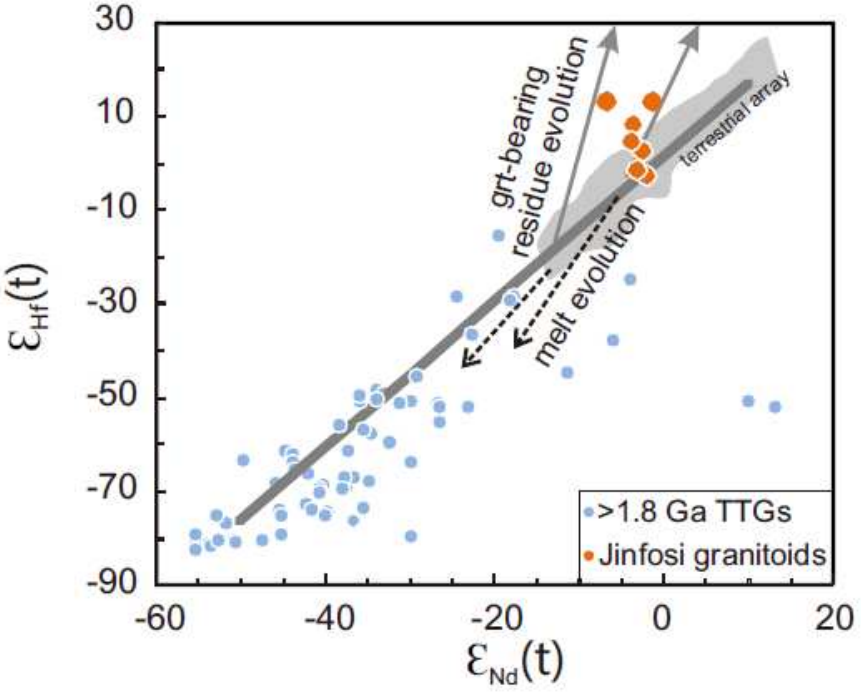

Fig. 6

Table 1: Whole-rock Sr-Nd-Hf-Pb isotopic data of samples from Jinfosi. Age corrected to 420 Ma.

	QL10-01	QL10-04	QL10-05	QL10-08	QL10-09	QL10-11	QL10-12
$^{176}Lu/^{177}Hf$	0.008	0.007	0.004	0.002	0.014	0.005	0.008
$^{176}Hf/^{177}Hf$	0.282921	0.282470	0.282891	0.282841	0.282580	0.282495	0.282686
2σ	9	10	12	7	8	6	9
$\varepsilon_{Hf}(420)$	12.64	-3.14	12.78	11.44	-1.14	-1.59	4.35
$^{147}Sm/^{144}Nd$	0.14	0.11	0.13	0.10	0.12	0.10	0.12
$^{143}Nd/^{144}Nd$	0.512406	0.512310	0.512109	0.512254	0.512250	0.512223	0.512232
2σ	9	9	12	12	10	8	9
$\varepsilon_{Nd}(420)$	-1.2	-1.9	-6.5	-3.4	-2.3	-3.1	-3.7
$^{87}Rb/^{86}Sr$	1.06	1.13	7.21	2.54	1.67	2.49	2.87
$^{87}Sr/^{86}Sr$	0.7114	0.7130	0.7485	0.7202	0.7184	0.7206	0.7237
$I_{Sr}(420)$	0.705	0.706	0.705	0.705	0.708	0.705	0.706
$^{206}Pb/^{204}Pb$	18.632	18.768	19.265	19.325	19.218	19.586	19.025
$^{207}Pb/^{204}Pb$	15.686	15.710	15.755	15.759	15.748	15.767	15.729
$^{208}Pb/^{204}Pb$	38.797	39.625	39.233	39.520	39.037	39.253	38.925
$^{208}Pb/^{204}Pb_i(420)$	38.35	38.52	38.56	38.61	38.44	38.62	38.45
$^{207}Pb/^{204}Pb_i(420)$	15.66	15.66	15.74	15.74	15.71	15.74	15.71
$^{206}Pb/^{204}Pb_i(420)$	18.21	17.94	19.03	18.97	18.62	19.16	18.69

$^{147}Sm/^{144}Nd_{CHUR0}$ =0.1967,$^{143}Nd/^{144}Nd_{CHUR0}$=0.512638, $\lambda(^{87}Rb)=1.42\times10^{-11}yr^{-1}$,$\lambda(^{147}Sm)=6.54\times10^{-12}yr^{-1}$

$^{176}Lu/^{177}Hf_{CHUR0}$=0.0332,$^{176}Hf/^{177}Hf_{CHUR0}$=0.282772, $\lambda(^{176}Lu)=1.93\times10^{-11}yr^{-1}$

$\varepsilon Hf\ (t)=[(^{176}Hf/^{177}Hf)sample(t)/(^{176}Hf/^{177}Hf)_{CHUR}(t)-1]*10^4$

$$(^{176}Hf/^{177}Hf)_{CHUR}(t)=(^{176}Hf/^{177}Hf)_{CHUR0}-(^{176}Lu/^{177}Hf)_{CHUR0}*(e^{\lambda t}-1)$$

Highlights:

The samples from the post-collisional Jinfosi Batholith show an inverse $\varepsilon_{Hf} - \varepsilon_{Nd}$ correlation.

Decoupled Nd and Hf isotopes are related to the depletion of HREEs.

The "garnet effect" is modelled and the modelling results require an ancient melt extraction with a large melting degree.

Melts complementary to the ancient melting residues may be recorded in some TTGs.